



The Obliquity of HIP 67522 b: A 17 Myr Old Transiting Hot, Jupiter-sized Planet

Alexis Heitzmann¹, George Zhou¹, Samuel N. Quinn², Stephen C. Marsden¹, Duncan Wright¹, Pascal Petit³, Andrew M. Vanderburg⁴, Luke G. Bouma⁵, Andrew W. Mann⁶, and Aaron C. Rizzuto⁷

¹ Centre for Astrophysics, University of Southern Queensland, West Street, Toowoomba, QLD 4350 Australia; alexis.heizmann@usq.edu.au

² Center for Astrophysics | Harvard & Smithsonian, 60 Garden Street, Cambridge, MA 02138, USA

³ Institut de Recherche en Astrophysique et Planétologie, Université de Toulouse, CNRS, CNES, 14 avenue Edouard Belin, F-31400 Toulouse, France

⁴ Department of Physics and Kavli Institute for Astrophysics and Space Research, Massachusetts Institute of Technology, 77 Massachusetts Avenue, Cambridge, MA 02139, USA

⁵ Department of Astrophysical Sciences, Princeton University, Princeton, NJ 08544, USA

⁶ Department of Physics and Astronomy, The University of North Carolina at Chapel Hill, Chapel Hill, NC 27599, USA

⁷ Department of Astronomy, The University of Texas at Austin, Austin, TX 78712, USA

Received 2021 September 9; revised 2021 October 26; accepted 2021 October 27; published 2021 November 12

Abstract

HIP 67522 b is a 17 Myr old, close-in ($P_{\text{orb}} = 6.96$ days), Jupiter-sized ($R = 10 R_{\oplus}$) transiting planet orbiting a Sun-like star in the Sco–Cen OB association. We present our measurement of the system’s projected orbital obliquity via two spectroscopic transit observations using the CHIRON spectroscopic facility. We present a global model that accounts for large surface brightness features typical of such young stars during spectroscopic transit observations. With a value of $|\lambda| = 5.8_{-5.7}^{+2.8\sigma}$ it is unlikely that this well-aligned system is the result of a high-eccentricity-driven migration history. By being the youngest planet with a known obliquity, HIP 67522 b holds a special place in contributing to our understanding of giant planet formation and evolution. Our analysis shows the feasibility of such measurements for young and very active stars.

Unified Astronomy Thesaurus concepts: Exoplanet astronomy (486); Exoplanet systems (484); Planetary alignment (1243); Planet formation (1241); Radial velocity (1332); Transit photometry (1709)

1. Introduction

One of the oldest puzzles in the field of exoplanets is the origin of short-orbit gas giants. With no equivalent in the solar system, it is far from obvious how these giant planets, orbiting their host star incredibly close (with orbital periods < 10 days), come to exist.

Among the observational properties easily measurable for these exoplanets when they transit, their sky-projected stellar obliquity (λ) angle may help differentiate between the multiple pathways explaining their origin (Dawson & Johnson 2018). Unfortunately, on its own, the obliquity angle cannot unambiguously identify a specific formation pathway. Star–planet tidal interactions, resulting in angular momentum exchanges between a host star and its planet, have the ability to circularize and shrink planetary orbits but also alter the star’s rotation axis alignment. This can erase primordial orbital characteristics (i.e., misalignments and/or eccentricity), preventing the identification of a specific migration channel. Because the timescales of such interactions span many orders of magnitudes (from 10^5 to 10^9 yr), the $\sim 150^8$ sky-projected orbital obliquity measurements obtained to date remain difficult to interpret (Triaud 2018; Albrecht et al. 2021).

Recently, it became possible to compare the obliquity distribution for very young stars (< 100 Myr) against that of more mature stars. These young planetary systems have not yet been influenced by star–planet tidal effects, and provide a glimpse into the primordial orbits of planets post-formation.

The recent efforts to characterize young planets discovered by the K2 and Transiting Exoplanet Survey Satellite (TESS; Ricker et al. 2016) missions, such as AU Mic b (Addison et al. 2021; Hirano et al. 2020; Martioli et al. 2020; Palle et al. 2020), V1298 Tau c (David et al. 2019; Feinstein et al. 2021), DS Tuc Ab (Montet et al. 2020; Zhou et al. 2020), and TOI 942 b (Wirth et al. 2021; Zhou et al. 2021), have the potential to deliver key insights on the formation and migration of close-in planets. Although these transiting planets orbiting rapidly rotating young stars are suitable candidates for obliquity measurements, their host stars’ young age imply that strong intrinsic variability needs to be dealt with in order to recover the true spin–orbit angles.

In this Letter we present a projected obliquity measurement for HIP 67522 b. This obliquity measurement is the first for a hot, Jupiter-sized planet younger than 100 Myr. With an age of only 17 Myr, HIP 67522 b has a radius of $10.178 \pm 0.440 R_{\oplus}$ (this work), a mass $< 5 M_J$ (Rizzuto et al. 2020), and is orbiting a bright ($V_{\text{mag}} = 9.876 \pm 0.026$) Sun-like star ($T_{\text{eff}} = 5675 \pm 75$ K).

We describe both photometric and spectroscopic observations of HIP 67522 b’s transits in Section 2 and present our combined model used to determine the projected obliquity of the system in Section 3. Finally, in Section 4, we place this measurement into context of other planetary systems around mature main-sequence stars.

2. Observations

2.1. TESS: Photometry

HIP 67522 b was first identified to transit in Sector 11 of the TESS primary mission (Rizzuto et al. 2020) over the period of 2019 April 22–May 21. The target was subsequently observed by TESS again during Sector 38 of the extended mission, over

⁸ TEPcat 2021 July (Southworth 2011).



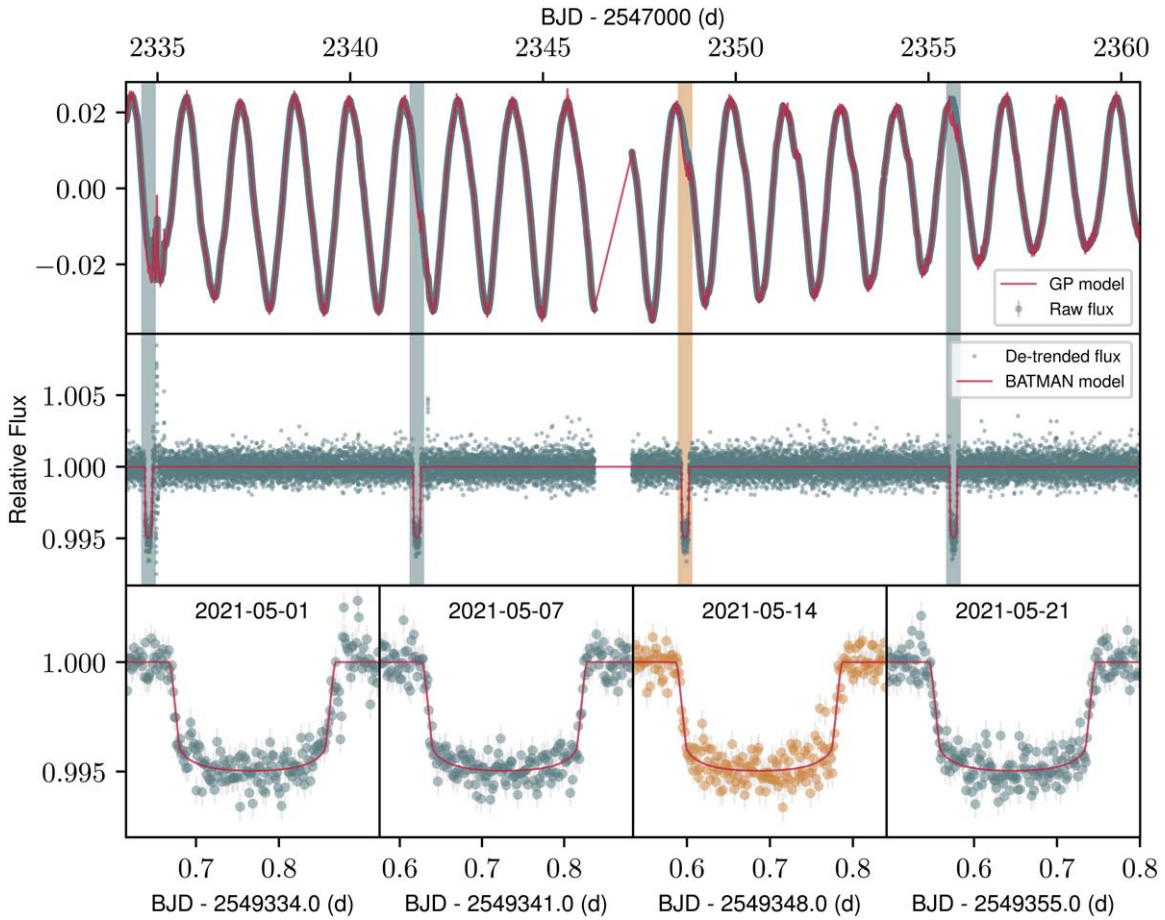


Figure 1. Top: TESS light curve for Sector 38. Data points are shown as gray points. The red line demonstrates the Gaussian process model describing the stellar variability of the TESS light curves. Locations of individual transit events are highlighted by the shaded regions. Middle: the TESS Sector 38 light curve after the Gaussian process model has been removed. Bottom: close-ups of each transit event. The transit event on 2021 May 14 was simultaneously observed by CHIRON, and is marked in orange for clarity.

the period of 2021 April 28–May 26. We make use of the Simple Aperture Photometry (Twicken et al. 2010, 2018; Morris et al. 2020) made available for the target star extracted by the Science Processing Observation Center (SPOC; Jenkins et al. 2016) from the target pixel files, obtained at a 2 minute cadence from both sectors of observations. The light curves were detrended against spacecraft motion via the quaternion detrending technique as per Vanderburg et al. (2019), allowing the recovery of two missing transits in the Sector 11 observations as shown in the discovery paper. Except for these two transits, the light curve was also decorrelated against the PDC band 3 (fast timescale) cotrending basis vectors, and modeled the rotation signal with a basis spline with breakpoints every 0.1 days while excluding points with transits from the systematics correction. This allowed the recovery of a systematic corrected light curve from Sector 38. The light curve from Sector 38 is shown in Figure 1.

2.2. CHIRON/SMARTS: Spectroscopy

We obtained two spectroscopic transits of HIP 67522 b with the CHIRON facility (Tokovinin et al. 2013). CHIRON is a high-resolution echelle spectrograph on the 1.5 m Small and Moderate Aperture Research Telescope System (SMARTS) telescope, located at Cerro Tololo Inter-American Observatory, Chile. CHIRON is fed via a fiber bundle, and has a spectral

resolving power of $\lambda/\Delta\lambda \equiv R \approx 80,000$ with a wavelength coverage from 4100 to 8700 Å.

A total of 24 observations, with exposure times of 1200 s each, were obtained on 2021 May 14, capturing the full transit and baselines on pre-ingress and post-egress from 2021 May 14 00:00 to 08:00 UTC. An additional partial transit was observed from 2021 June 17 23:15 to 2021 June 18 05:20 UTC, with a total of 18 observations at 1200 s integration time each. The stellar spectra were extracted via the official CHIRON pipeline (Paredes et al. 2021), with wavelength calibration provided by a set of thorium–argon cathode ray lamp exposures that bracket each transit sequence. To derive line-broadening profiles from each spectrum, we perform a least-squares deconvolution of the observed spectrum against a set of synthetic nonrotating spectral templates (Donati et al. 1997; Collier Cameron et al. 2010), making use of the ATLAS9 atmosphere models (Castelli & Kurucz 2003) computed at the atmospheric parameters of HIP 67522 ($T_{\text{eff}} = 5725$ K, $\log g = 4.0$, and $[\text{Fe}/\text{H}] = 0$). To ensure realistic uncertainties on our measurement of λ , we rebinned these line profiles to the velocity dispersion corresponding to the detector’s pixel size. We make use of these for the transit spectroscopic modeling as described in Section 3.2. In addition, we also model each line profile with a kernel that incorporates the effects of rotational, macro-turbulent, and instrumental line broadening. We make use of this model to determine the rotational broadening velocity

$v \sin i_*$ necessary for the line profile modeling, measuring a rotational broadening velocity of $v \sin i_* = 50 \pm 3 \text{ km s}^{-1}$, consistent with that of $54.2 \pm 0.7 \text{ km s}^{-1}$ reported in the discovery paper from an ensemble of spectroscopic observations.

3. Analysis

The very young age of HIP 67522 goes hand in hand with substantial intrinsic stellar variability in both spectroscopic and photometric observations, with 2%–3% variations seen in both TESS Sector 11 and 38 light curves. The variability seen for HIP 67522 can be mostly attributed to surface brightness features (spots and plages). We develop a model below that incorporates both photometric (Section 3.1) and spectroscopic (Section 3.2) transits as well as spot modeling to deal with the influence of stellar activity on our projected obliquity measurements.

3.1. Transit Photometry

A total of eight transits, four in Sector 11 and four in Sector 38, were observed by TESS. The TESS photometry exhibits significant stellar rotational variability due to the youth of the host star. We apply a Gaussian process model to account for this variability. We model the light curve using a stochastically driven simple harmonic oscillation kernel as is implemented in the CELERITE package (Foreman-Mackey et al. 2017), with free parameters describing its amplitude S_0 and damping coefficient Q . We fixed the frequency $\omega_0 = 1/P_{\text{rot}} = 1/1.39$ (see the last paragraph of Section 3.2 for justification). We also simultaneously model the planetary transit using the BATMAN package (Kreidberg 2015), including free parameters describing the transit centroid timing T_c , orbital period P_{orb} , radius ratio R_p/R_* , normalized semimajor axis a/R_* , and the line-of-sight inclination of the transit i . Following the low eccentricity found in Rizzuto et al. (2020), the orbit is assumed to be circular for this model.

The light-curve and best-fit model for the Sector 38 observations are shown in Figure 1. We subtract the Gaussian process model from the TESS observations, and pass the resulting detrended light curve to the subsequent analysis described in Section 3.3.

3.2. Transit Spectroscopy

Any phenomenon introducing brightness variations on the stellar disk that are asymmetric will leave rotationally modulated imprints on the observed spectroscopic line profiles. As these variations move across the stellar disk, they block/enhance incoming flux at a wavelength (and corresponding radial velocity) depending on their longitude. This is because light emitted by different parts of the stellar disk experience a different Doppler shift due to the star’s rotation. This directly translates into bumps and dips on the rotational line profiles. Doppler tomography consists of monitoring the evolution of line profiles during a planetary transit to catch the distortions induced by the eclipsing body, called the “Doppler shadow”. The way this Doppler shadow crosses the line profiles over time yields the angle at which the planet crosses the stellar disk, the projected spin–orbit angle λ . Any other brightness variations (i.e., spot-induced features in a first approximation) will contribute to distort the line profiles in a similar fashion.

Table 1
Global Model Parameters

Parameters	Prior ^a	Results
Transit		
T_c (BJD _{TDB})	\mathcal{U}	$1604.023722^{+0.00024}_{-0.00023}$
P_{orb} (days)	\mathcal{U}	$6.959471^{+0.0000030}_{-0.0000030}$
R_p (R_*)	\mathcal{U}	$0.067471^{+0.00019}_{-0.00017}$
a (R_*)	\mathcal{U}	$11.685^{+0.112}_{-0.220}$
i ($^\circ$)	$\mathcal{U}[86,90]$	$89.23^{+0.37}_{-0.47}$
e	0 (fixed)	...
μ_1	0.148 (fixed) ^b	...
μ_2	0.23 (fixed) ^b	...
Doppler Tomography		
$v \sin i_*$ (km s^{-1})	$\mathcal{G}[50,1]$	$49.21^{+0.95}_{-0.97}$
λ ($^\circ$)	\mathcal{U}	$-5.8^{+2.8}_{-5.7}$
v_{macro} (km s^{-1})	\mathcal{U}	$0.59^{+0.43}_{-0.41}$
ν_1	0.4139 (fixed) ^c	...
ν_2	0.2494 (fixed) ^c	...
#spots	1 (fixed)	...
θ_{spot1} ($^\circ$)	\mathcal{U}	$212.95^{+0.36}_{-0.37}$
ϕ_{spot1} ($^\circ$)	$\mathcal{U}[0,90]$	$57.8^{+2.7}_{-2.2}$
R_{spot1} ($^\circ$)	\mathcal{U}	$4.76^{+0.24}_{-0.71}$
T_{spot1} (K)	$\mathcal{U}[0.6 \times T_{\text{eff}}, 0.8 \times T_{\text{eff}}]$	3890^{+288}_{-1550}
P_{rot} (days)	1.39 (fixed)	...
Light-curve GP		
$\log S_0$	\mathcal{U}	$-1.6^{+0.4}_{-3.7}$
$\log Q$	\mathcal{U}	$3.37^{+0.67}_{-0.77}$
$\log \omega_0$	-0.329 (fixed)	...
Derived Parameters		
R_p (R_{\oplus})	...	10.178 ± 0.440
R_p (R_J)	...	0.928 ± 0.040
3D obliquity ($^\circ$)	...	$20.2^{+10.3}_{-8.7}$
i_* ($^\circ$)	...	>85 (3σ)

Notes.

^a \mathcal{U} unconstrained uniform priors; $\mathcal{U}[a, b]$ constrained uniform priors with boundaries a and b ; $\mathcal{G}[\mu, \sigma]$ Gaussian priors.

^b Adopted at the TESS band from Claret (2017).

^c Adopted at the V band from Claret et al. (2012).

We therefore modeled both contribution (spots and planet) to fit the observed line profiles and recover λ .

The star was modeled as a circular mask on a grid of pixels, each with a value between 0 and 1 representing fractional brightness f_b . The mask is a combination of (i) a uniform disk ($f_b = 1$), (ii) a limb-darkening quadratic law parameterized with a linear ν_1 and a quadratic ν_2 coefficient (given in Table 1), (iii) the spot(s), and (iv) the transiting planet. Spots were modeled as spherical caps defined by their colatitude (complementary angle of latitude, i.e., 0° at the north pole and 180° at the south pole) ϕ , longitude θ , angular radius R_{spot} , and temperature T_{spot} conditioning their brightness, as per

$$f_b = (T_{\text{spot}}/T_{\text{eff}})^4. \quad (1)$$

The projection of each spot on the stellar disk was then computed analytically and its contribution was added to the total mask. Finally, the transiting planet was assumed on a circular orbit and modeled as a disk ($f_b = 0$). Its shadow on the stellar disk was parameterized by T_c , P_{orb} , R_p/R_* , a/R_* , ω , i , and λ (see the values in Table 1).

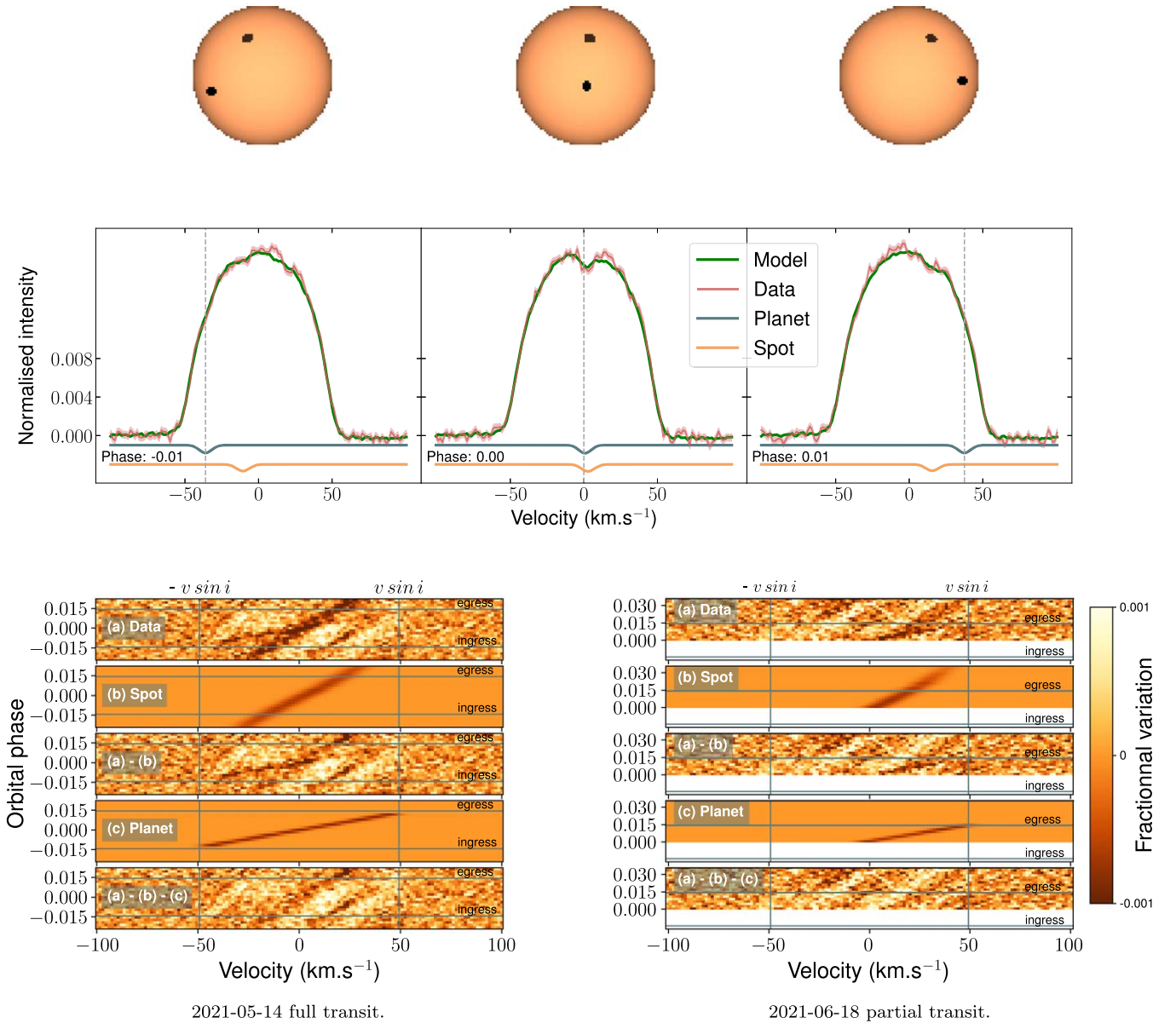


Figure 2. Results from the spectroscopic transit modeling of HIP 67522 b. Top: modeled stellar disk including a single spot and the transiting planet at phase -0.01 (left), 0 (center), and 0.01 (right). Middle: line profiles fit matching the above images. Observed line profiles are shown in red with uncertainties in lighter red. Fit to the data (mean line profile + integrated modeled stellar disk) is shown in green, the planet contribution in blue, and the spot contribution in orange. Gray vertical dotted lines express planet transit phases. Bottom: result plots for the 2021 May 14 full transit (left) and the 2021 June 18 partial transit (right). Each subpanel shows the variation of lines profiles in velocity space (horizontal axis) for different orbital phases of HIP 67522 b (vertical axis). (a) Residuals between each observed line broadening and the mean observed line profile. (b) Spot-only model. (a)–(b) Line profile residuals after subtraction of the spot model; we see that the spot signature has been removed, leaving a clear planetary signature. (c) Modeled planet. (a)–(b)–(c) Residuals after subtraction of both the spot and planet model. Horizontal black lines show the phase of transit ingress (bottom) and egress (top). Vertical black lines are $-v \sin i$ (left) and $+v \sin i$ (right).

To obtain the full disk-integrated line profiles, we summed the pixels along the vertical axis of the stellar disk (i.e., for each radial velocity bin). Finally, we incorporate line broadening in the observations via a convolution of our model with a Gaussian kernel, with the width being the quadrature addition of the instrumental resolution and the macroturbulent velocity (v_{macro}).

A dark spot feature was seen during both spectroscopic transits on 2021 May 14 and 2021 June 18 (Figure 2). We interpret this to be the same spot feature. That it reappears at the same location on the second transit is interpreted to be that the planet orbital period is a multiple of the rotation period, near 5:1 resonance. This is supported by the near-sinusoidal light-

curve variability seen during Sector 38 of the TESS observations. We therefore adopt a fixed stellar rotation period of $P_{\text{rot}} = 1.39$ days for both the Gaussian process detrending and our Doppler tomographic analysis, and assume that there is one fixed long-lived spot that does not vary in size or temperature between the two observations. Not taking into account the spot evolution explains the slight residuals left after removal of the main spot feature as seen on the bottom panel of Figure 2 (panels (a)–(b) and (a)–(b)–(c)). For reference, a Lomb–Scargle analysis of the joint Sector 11 and 38 light curves reveals a rotation period of 1.4 ± 0.1 day, in agreement with the value we adopt in this analysis.

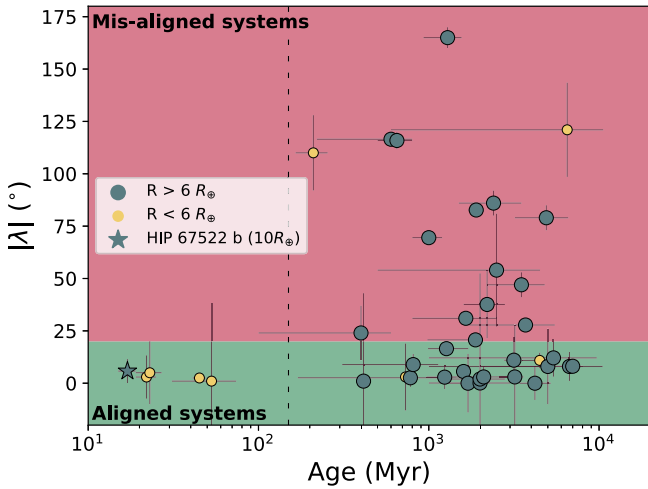


Figure 3. Systems younger than 10 Gyr that have both their age (NASA Exoplanet Archive 2021 July) and obliquity constrained. Yellow smaller circles represent Neptune-sized planets ($R < 6 R_{\oplus}$), larger blue circles show Jupiter-sized planets ($R > 6 R_{\oplus}$), and the blue star symbolizes HIP 67522 b. The very young systems (< 100 Myr) are, in ascending order of age, HIP 67522, AU Mic, V1298 Tau, DS Tuc A, and TOI 942. The red and green areas show aligned ($|\lambda| < 20^\circ$) and misaligned ($|\lambda| > 20^\circ$) systems, respectively.

3.3. Global Fit

We simultaneously fitted the transit light curves modeled with BATMAN (Section 3.1) to the TESS data and the line profiles obtained through our Doppler tomographic model to the least-squares deconvolution profiles (Section 3.2).

For a given parameter set, we computed the likelihood for both the photometric and spectroscopic data sets. To determine the best-fitting parameter values and resulting posteriors, we made use of a Markov Chain Monte Carlo analysis using the affine-invariant ensemble sampler EMCEE (Foreman-Mackey et al. 2013). The analysis included 240 simultaneous chains with 10000 iterations each. The resulting posteriors are presented in Table 1. We derived a planet radius of $10.178 \pm 0.44 R_{\oplus}$, agreeing with the previous value of $10.07 \pm 0.47 R_{\oplus}$ from Rizzuto et al. (2020). We note that the availability of four extra transits did not improve the uncertainty on R_p , limited by the poorer constraint on R_* .

4. Conclusions

We measured the projected obliquity angle of HIP 67522 b to be $|\lambda| = 5.8^{+2.8}_{-5.7}^\circ$. With a stellar inclination estimated following Masuda & Winn (2020), we derived the 3D obliquity to be $\psi = 20.2^{+10.3}_{-8.7}^\circ$. At an age of 17 Myr, HIP 67522 b is the youngest planet to receive such characterization. We demonstrate that a precise measurement of the sky-projected obliquity is possible for such young stars, despite the activity-dominated spectroscopic transit observations. Our single-spot model allows us to unambiguously disentangle the planetary signature from the stellar activity.

Figure 3 places HIP 67522 b into context of other planetary systems that have known obliquities and constrained ages.⁹ This particular system joins AU Mic b (Palle et al. 2020; Addison et al. 2021; Hirano et al. 2020; Martioli et al. 2020), V1298 Tau c (David et al. 2019; Feinstein et al. 2021), DS Tuc Ab (Newton et al. 2019; Montet et al. 2020; Zhou et al. 2020),

and TOI 942 b (Wirth et al. 2021) in the group of systems younger than 100 Myr old that have their obliquity measured. Remarkably, all these systems have been found to be on well-aligned orbits, encouraging the pursuit of very young star obliquity measurements to confirm this trend.

With a radius of $10 R_{\oplus}$, HIP 67522 b is the only hot, Jupiter-sized planet in this very young group of systems. Its future evolution is still unclear, however, and the lack of constraint on its mass prevents us from definitively classifying it as a proto-hot Jupiter. Super-Earths and Neptune-sized planets commonly found around Sun-like stars can have a radii of $\sim 10 R_{\oplus}$ at the age of HIP 67522. The planet is undergoing Kelvin–Helmholtz contraction and photoevaporation, and its eventual radius depends strongly on its core-envelope makeup (e.g., Lopez & Fortney 2013).

If HIP 67522 b is indeed a proto-hot Jupiter, it is a prime example of one that did not migrate via high-eccentricity pathways. The circularization of HIP 67522 b’s orbit is on the Gyr timescale (estimated from Goldreich & Soter 1966), playing against a high-eccentricity-type migration. Classic planet systems such as HD 80606 b (Naef et al. 2001; Wu & Murray 2003; Pont et al. 2009; Hébrard et al. 2010) and HD 17156 b (Barbieri et al. 2007; Cochran et al. 2008; Narita et al. 2008) exhibit highly eccentric and oblique orbits. For most other mature hot Jupiters, though, it is more difficult to decipher their original migration pathways due to tidal synchronization that occurs at the hundreds of millions of years to gigayear timescales (e.g., Lai 2012; Valsecchi & Rasio 2014), erasing evidence of their primordial histories. HIP 67522 b may be the first such example for which the most likely explanation is that the primordial orbit of a close-in Jovian planet is well aligned. Recently, Albrecht et al. (2021) found that hot Jupiters are preferentially found in well-aligned or polar orbits. There are a range of mechanisms that can result in such bimodality in the obliquity distribution, and understanding the age–obliquity distribution can help distinguish between these mechanisms. For example, magnetic warping of the protoplanet disk can result in hot Jupiters that formed in situ being found in oblique orbits (e.g., Lai et al. 2011). With more observations, a prevalence of well-aligned hot Jupiters around young stars may help limit the real-life effectiveness of such pathways.

If HIP 67522 b does become a Neptune-sized planet, it adds to the well-aligned pool of very young systems, contrasting with the often misaligned single-planet Neptune-like systems in close orbit around more mature aged stars. Even with a mass of a few $10 M_{\oplus}$, the circularization timescale is likely on the few 100 Myr timescale, one order of magnitude older larger than the age of the system, disfavoring high-eccentricity migration. HIP 67522 b would contribute to the growing interest to understand the formation of close-in Neptunes (e.g., Bean et al. 2021) and to make sense of the alignment distribution of these commonly found exoplanets.

Although not seen in Sector 38, HIP 67522 b has a possible nearby exterior transiting companion with an orbital period of > 23 days (Rizzuto et al. 2020). The existence of HIP 67522 c is tentative, but if confirmed, HIP 67522 b would be a more consistent future Neptune-sized planet as hot Jupiters are rarely found with outer companions. Dynamical interactions within closely packed planetary systems can excite mutual inclinations (Hansen & Murray 2013), and often result in the destruction of the interior planetary architecture if the outer companion is

⁹ NASA Exoplanet Archive 2021 July.



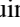

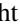

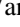
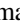
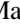

massive (Huang et al. 2017). Systems like HIP 67522 and V1298 Tau (David et al. 2019; Feinstein et al. 2021) are candidates to test planet–planet interactions before planetary systems have settled into their final stable forms.

This research has been supported by an Australian Government Research Training Program Scholarship. G.Z. thanks the support of the ARC DECRA program DE210101893. G.Z. thanks the support of the TESS Guest Investigator Program G03007. This research has used data from the CTIO/SMARTS 1.5 m telescope, which is operated as part of the SMARTS Consortium by RECONS members Todd Henry, Hodari James, Wei-Chun Jao, and Leonardo Paredes. At the telescope, observations were carried out by Roberto Aviles and Rodrigo Hinojosa. In the scope of this research, we used the University of Southern Queensland’s (USQ) *Fawkes HPC* which is co-sponsored by the Queensland Cyber Infrastructure Foundation (QCIF). This research has made use of the NASA Exoplanet Archive, which is operated by the California Institute of Technology, under contract with the National Aeronautics and Space Administration under the Exoplanet Exploration Program. Funding for the TESS mission is provided by NASA’s Science Mission directorate. We acknowledge the use of public TESS Alert data from pipelines at the TESS Science Office and at the TESS Science Processing Operations Center. This research has made use of the Exoplanet Follow-up Observation Program website, which is operated by the California Institute of Technology, under contract with the National Aeronautics and Space Administration under the Exoplanet Exploration Program. This paper includes data collected by the TESS mission, which are publicly available from the Mikulski Archive for Space Telescopes (MAST). Resources supporting this work were provided by the NASA High-End Computing (HEC) Program through the NASA Advanced Supercomputing (NAS) Division at Ames Research Center for the production of the SPOC data products.

Facilities: CTIO:1.5 m, TESS.

Software: ASTROPY (Astropy Collaboration et al. 2013, 2018), BATMAN (Kreidberg 2015), CELERITE (Foreman-Mackey et al. 2017), EMCEE (Foreman-Mackey et al. 2013).

ORCID iDs

Alexis Heitzmann  <https://orcid.org/0000-0002-8091-7526>
 George Zhou  <https://orcid.org/0000-0002-4891-3517>
 Samuel N. Quinn  <https://orcid.org/0000-0002-8964-8377>
 Stephen C. Marsden  <https://orcid.org/0000-0001-5522-8887>
 Duncan Wright  <https://orcid.org/0000-0001-7294-5386>
 Pascal Petit  <https://orcid.org/0000-0001-7624-9222>
 Andrew M. Vanderburg  <https://orcid.org/0000-0001-7246-5438>
 Luke G. Bouma  <https://orcid.org/0000-0002-0514-5538>
 Andrew W. Mann  <https://orcid.org/0000-0003-3654-1602>
 Aaron C. Rizzuto  <https://orcid.org/0000-0001-9982-1332>

References

- Addison, B. C., Horner, J., Wittenmyer, R. A., et al. 2021, *AJ*, 162, 137
 Albrecht, S. H., Marcussen, M. L., Winn, J. N., Dawson, R. I., & Knudstrup, E. 2021, *ApJL*, 916, L1
 Astropy Collaboration, Robitaille, T. P., Tollerud, E. J., et al. 2013, *A&A*, 558, A33
 Astropy Collaboration, Price-Whelan, A. M., Sipőcz, B. M., et al. 2018, *AJ*, 156, 123
 Barbieri, M., Alonso, R., Laughlin, G., et al. 2007, *A&A*, 476, L13
 Bean, J. L., Raymond, S. N., & Owen, J. E. 2021, *JGRE*, 126, e06639
 Castelli, F., & Kurucz, R. L. 2003, in IAU Symp. 210, Modelling of Stellar Atmospheres, ed. N. Piskunov et al. (Cambridge: Cambridge Univ. Press)
 Claret, A. 2017, *A&A*, 600, A30
 Claret, A., Hauschildt, P. H., & Witte, S. 2012, *A&A*, 546, A14
 Cochran, W. D., Redfield, S., Endl, M., & Cochran, A. L. 2008, *ApJL*, 683, L59
 Collier Cameron, A., Guenther, E., Smalley, B., et al. 2010, *MNRAS*, 407, 507
 David, T. J., Petigura, E. A., Luger, R., et al. 2019, *ApJL*, 885, L12
 Dawson, R. I., & Johnson, J. A. 2018, *ARA&A*, 56, 175
 Donati, J.-F., Semel, M., Carter, B. D., Rees, D. E., & Collier Cameron, A. 1997, *MNRAS*, 291, 658
 Feinstein, A. D., Montet, B. T., Johnson, M. C., et al. 2021, *AJ*, 162, 213
 Foreman-Mackey, D., Agol, E., Ambikasaran, S., & Angus, R. 2017, *AJ*, 154, 220
 Foreman-Mackey, D., Hogg, D. W., Lang, D., & Goodman, J. 2013, *PASP*, 125, 306
 Goldreich, P., & Soter, S. 1966, *Icar*, 5, 375
 Hansen, B. M. S., & Murray, N. 2013, *ApJ*, 775, 53
 Hébrard, G., Désert, J. M., Díaz, R. F., et al. 2010, *A&A*, 516, A95
 Hirano, T., Krishnamurthy, V., Gaidos, E., et al. 2020, *ApJL*, 899, L13
 Huang, C. X., Petrovich, C., & Deibert, E. 2017, *AJ*, 153, 210
 Jenkins, J. M., Twicken, J. D., McCauliff, S., et al. 2016, *Proc. SPIE*, 9913, 99133E
 Kreidberg, L. 2015, *PASP*, 127, 1161
 Lai, D. 2012, *MNRAS*, 423, 486
 Lai, D., Foucart, F., & Lin, D. N. C. 2011, *MNRAS*, 412, 2790
 Lopez, E. D., & Fortney, J. J. 2013, *ApJ*, 776, 2
 Martioli, E., Hébrard, G., Moutou, C., et al. 2020, *A&A*, 641, L1
 Masuda, K., & Winn, J. N. 2020, *AJ*, 159, 81
 Montet, B. T., Feinstein, A. D., Luger, R., et al. 2020, *AJ*, 159, 112
 Morris, R. L., Twicken, J. D., Smith, J. C., et al. 2017, in Kepler Data Processing Handbook: Photometric Analysis (KSCI-19081-003) ed. J. M. Jenkins (Mountain View, CA: NASA Ames Research Center)
 Naef, D., Latham, D. W., Mayor, M., et al. 2001, *A&A*, 375, L27
 Narita, N., Sato, B., Ohshima, O., & Winn, J. N. 2008, *PASJ*, 60, L1
 Newton, E. R., Mann, A. W., Tofflemire, B. M., et al. 2019, *ApJL*, 880, L17
 Palle, E., Oshagh, M., Casasayas-Barris, N., et al. 2020, *A&A*, 643, A25
 Paredes, L. A., Henry, T. J., Quinn, S. N., et al. 2021, *AJ*, 162, 176
 Pont, F., Hébrard, G., Irwin, J. M., et al. 2009, *A&A*, 502, 695
 Ricker, G. R., Vanderspek, R., Winn, J., et al. 2016, *Proc. SPIE*, 9904, 99042B
 Rizzuto, A. C., Newton, E. R., Mann, A. W., et al. 2020, *AJ*, 160, 33
 Southworth, J. 2011, *MNRAS*, 417, 2166
 Tokovinin, A., Fischer, D. A., Bonati, M., et al. 2013, *PASP*, 125, 1336
 Triard, A. H. M. J. 2018, in Handbook of Exoplanets, ed. H. J. Deeg & J. A. Belmonte (Berlin: Springer), 1375
 Twicken, J. D., Clarke, B. D., Bryson, S. T., et al. 2010, *Proc. SPIE*, 7740, 774023
 Twicken, Joseph D., Catanzarite, Joseph H., Clarke, Bruce D., et al. 2018, *PASP*, 130, 064502
 Valsecchi, F., & Rasio, F. A. 2014, *ApJ*, 786, 102
 Vanderburg, A., Huang, C. X., Rodriguez, J. E., et al. 2019, *ApJL*, 881, L19
 Wirth, C. P., Zhou, G., Quinn, S. N., et al. 2021, *ApJL*, 917, L34
 Wu, Y., & Murray, N. 2003, *ApJ*, 589, 605
 Zhou, G., Winn, J. N., Newton, E. R., et al. 2020, *ApJL*, 892, L21
 Zhou, G., Quinn, S. N., Irwin, J., et al. 2021, *AJ*, 161, 2